Electron paramagnetic centers in donor-doped CaTiO3 single crystals

Electron paramagnetic centers in donor-doped $CaTiO_3$ single crystals

K. Ueda, H. Kawazoe,* and H. Hosono
Materials and Structures Laboratory, Tokyo Institute of Technology, 4259 Nagatsuta, Midori, Yokohama 226-8503, Japan
(Received 17 August 1999; revised manuscript received 21 October 1999)

Electron spin resonance signals observed in donor-doped $CaTiO_3$ single crystals ($Ca_{1-x}Y_xTiO_3$ or $CaTi_{1-x}Nb_xO_3$) were analyzed and the results were discussed from a viewpoint of carrier generation. Several types of signals were observed in insulating samples, and they were tentatively assigned to some acceptors such as Al impurity and the defects relating oxygen excess. Two types of signals with sharp and broad features, both of which are assignable to electron-trapped-type centers, were observed in conductive samples. The origins of the sharp and broad signals were attributed to electrons tightly trapped on Ti^{4+} ions and electrons loosely localized around donors, respectively, from analysis of angular and temperature dependence of the signals. The concentrations of the centers for the sharp and broad signals were estimated at ~3 K to be $\sim 3\times10^{18}$ cm^{-3} in the H_2-reduced samples with $x=10^{-4}$ and $\sim 3\times10^{19}$ cm^{-3} in the as-prepared samples with $x=10^{-2}$, respectively. Although no obvious correlation between electroconductive behavior and signal intensity was observed for the sharp signals, intensities of the broad signal increased as the electroconductive behavior turned from metallic to semiconducting below ~25 K. Therefore, it was found that the electrons responsible for the broad signals convert into conduction electrons when they are thermally released at high temperatures, and their concentration is high enough to influence the electroconductive behavior.

I. INTRODUCTION

Alkaline earth titanates, $MTiO_3$ (M=Ca,Sr,Ba), are known as insulating or dielectric oxide materials in stoichiometric states. However, it is well recognized that these materials become *n*-type electrical conductors by donor-doping.[1–6] The donor-doped conducting materials are in practical uses such as resistors, thermistors, and sensors. Donors are usually introduced into the materials by cation substitution or reduction treatment, which generates oxygen vacancies. The technique of doping is a key process in the application of these materials.

We have studied electronic transport properties of nondoped and donor-doped $CaTiO_3$ single crystals for the total understanding of their semiconducting properties. For this purpose, examinations of the electrical conductivity, electronic structure of the material and electronic states of donors are required. Analysis of the electroconductive properties and electronic structure of $CaTiO_3$ have been already carried out and the results were published elsewhere.[1,7,8] Analysis of the electronic states of donors and their influence on the electrical conductivity will be reported in the present paper. Finding a correlation between the electronic states of donors and electroconductive properties of the materials is essential in the analysis, because the donors that contribute to the generation of conduction electrons are practically of importance for the control of the electrical conductivity. Since oxide semiconductors, including the alkaline earth titanates, are polar or ionic materials, the way of local lattice relaxation around the dopants and the change in the valence states of dopants in the oxide semiconductors are expected to be different from those in the conventional semiconductors.

Several studies on the electronic structures of the alkaline earth titanates were carried out on the basis of theoretical calculations like an energy band calculation and experimental estimations by normal and inverse photoemission spectroscopy.[7–18] These studies revealed that the bottom of the conduction band is mainly formed by a Ti 3*d* band in the titanates and electrons generated by donor-doping occupy the bottom of the conduction band. On the other hand, studies on the electronic states of dopants are not so extensively undertaken as those on electronic structures. Although there were some examinations about paramagnetic centers in the alkaline earth titanates, most of them concentrate on the phase transition of the materials, photochromism or spectroscopic features of the centers such as transition metal ions.[19–29] Therefore, the studies about the electronic states of dopants and their effects on electroconductive properties are limited.

Some researchers have reported Fe, Cr, and Mn-related centers in $SrTiO_3$ and $BaTiO_3$ which can act as acceptors. Regarding other acceptors, Ensign and Stokowski have found an Al^{3+} center,[30] and Schirmer *et al.* have resolved another Al^{3+} center in $SrTiO_3$.[31] Varnhorst *et al.* have resolved various O^- centers associated with alkali ions in $BaTiO_3$.[32] On the other hand, as for donors, van Engelen and Henning have detected a Ti^{3+} center in $SrTiO_3$,[33] and Scharfschwerdt *et al.*, Possenriede *et al.* and Takeda *et al.* have found Ti^{3+} centers in $BaTiO_3$.[34–36] Although a Nb^{4+} center has been clearly observed in rutile,[37] detection of donors like La and Nb ions in the alkaline earth titanates has not been reported so far except the study by Possenriede *et al.*[35] Most of these studies do not deal with the electrical conductivity of samples directly. Accordingly, it seems that correlations between the electronic states of donors and carrier generation by donor doping have not been understood well in these materials yet.

The purpose of the present study is observation of electron spin resonance (ESR) signals in Y- or Nb-doped $CaTiO_3$ single crystals and their assignment from the results of not only ESR but also electrical conductivity measurements. It is well known that ESR is a useful and sensitive technique for the observation of electronic states of localized spins. The

dopants, Y and Nb, under nonionized states can be paramagnetic centers in $CaTiO_3$ if they substitute Ca and Ti ions, respectively. Therefore, ESR measurements on nondoped and Y- or Nb-doped $CaTiO_3$ single crystals were carried out with the examination of correlations between ESR signals and electrical conductivity.

II. EXPERIMENT

Single crystals were used as samples to avoid the effects of grain boundaries on carrier transport and carrier generation or compensation. Samples, non-doped and donor-doped $CaTiO_3$ single crystals were prepared by a floating zone method using an infrared furnace. Details of sample preparations were described in the previous paper.[1]

Y and Nb ions were selected as donors so that these ions are known to substitute Ca and Ti ions, respectively. The composition of the crystals is nominally expressed by $Ca_{1-x}Y_xTiO_3$ or $CaTi_{1-x}Nb_xO_3$ ($x=0$, 10^{-4}, 10^{-3}, and 10^{-2}). H_2 reduction treatments were carried out on insulating samples with $x=0$, 10^{-4}, and 10^{-3} to induce electrical conduction. The samples were annealed in H_2 flow at 600, 800, or 1000 °C for 6 h.

Electrical conductivities of the as-prepared crystals with $x=10^{-2}$ were measured at low temperatures. Temperature dependence of the electrical conductivities was monitored by the dc four-probe method in the temperature range from 1.6 to 273 K. Samples were cut out in a shape of a rod about 5 mm long, and ohmic electrodes were attached to them using Ag-Zn paste.

ESR measurements were performed in the temperature range from ~3 K to room temperature using an *X*-band spectrometer (Bruker ESP 300E) with a dual cavity and goniometer. The spectrometer was operated with microwave frequency ~9.66 GHz and modulation field 0.1~0.2 mT. The *g* values of signals were calibrated by using the signal of DPPH ($g=2.0036$) in the rear cavity without changing a sample position. The concentrations of paramagnetic centers were estimated from their signal intensities in comparison with the signal intensity of Cu^{2+} in $CuSO_4 \cdot 5H_2O$.

Samples for the measurements of powder patterns were prepared by crushing and grinding single crystals. Crystals used for the observation of angular variations in resonance magnetic field were cut in a shape of a rectangular rod with the sides ~2 mm so that the surface planes of the crystals become perpendicular to the crystal axes, referring to Laue photographs. The crystals were fixed at the edge of a quartz glass rod and rotated in the cavity by a goniometer. (In the present paper, *a*, *b*, and *c* axes of $CaTiO_3$ are taken in the space group, Pbnm, in which the lattice constants satisfy $a<b<c$.[38])

III. RESULTS

A. Electrical conductivity

Only the crystals with dopant concentration $x=10^{-2}$ were electroconductive and showed metallic behavior in the as-prepared states, as described in the previous paper.[1] The other crystals with lower dopant concentrations $x=0$, 10^{-4}, and 10^{-3} were insulating at room temperature or slightly *p*-type conductive at high temperatures, probably due to unexpected impurities such as Al^{3+} ions at Ti^{4+} sites or oxygen excess caused by deviation of cation ratio, Ca/Ti. However, upon the H_2 reduction, the donor-doped samples with $x=10^{-4}$ and 10^{-3} showed a drastic change from insulators to *n*-type electrical conductors and metallic behavior at room temperature. These phenomena are not dependent on donor species, that is, the results on Y-doped samples are similar to those on Nb-doped samples.

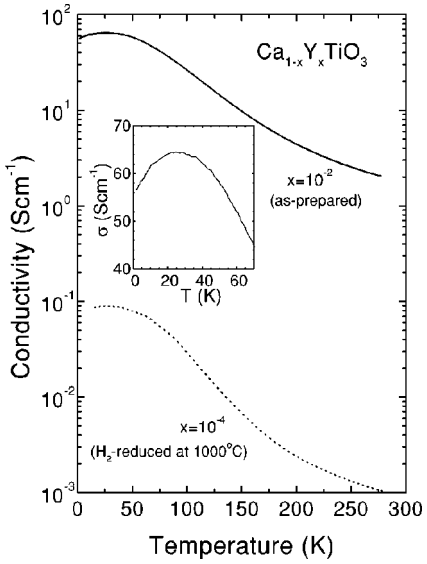

FIG. 1. Temperature dependence of electrical conductivity in the as-prepared single crystal of $Ca_{1-x}Y_xTiO_3$ with $x=10^{-2}$ (solid line) and the H_2-reduced crystal with $x=10^{-4}$ (dotted line). Inset magnifies the electrical conductivity of the $x=10^{-2}$ crystal below 70 K in the linear scale of the conductivity.

Figure 1 shows the electrical conductivity of the as-prepared sample of $x=10^{-2}$ Y concentration and the H_2-reduced sample of $x=10^{-4}$ at low temperatures. (The data for the $x=10^{-4}$ sample was taken from the previous paper.[1]) Metallic behavior was observed in the temperature range from 273 to ~25 K in these samples. On the other hand, semiconducting behavior obviously showed up below ~25 K in the $x=10^{-2}$ sample. Therefore, it becomes evident that the electroconductive behavior in the as-prepared sample with $x=10^{-2}$ Y concentration varies from metallic to semiconducting at ~25 K as temperature decreases.

B. ESR signals

1. General features

The single crystals of $x=0$, 10^{-4}, and 10^{-3}, which are insulating in the as-prepared states, showed many and fairly complicated signals. Although sharp signals, supposedly related to Fe^{3+} ions, were observed, the other signals were too complex to be analyzed. Dependence of the signal intensities on microwave power or that of the resonance fields on crystal orientation with respect to magnetic field was checked for their separation and classification. Nevertheless, the attempt was unsuccessful and the analysis of the complicated signals has been suspended. It should be noted, however, that the complicated signals were observed in both the nondoped and donor-doped samples with low dopant concentration only when the samples were insulating at room temperature.

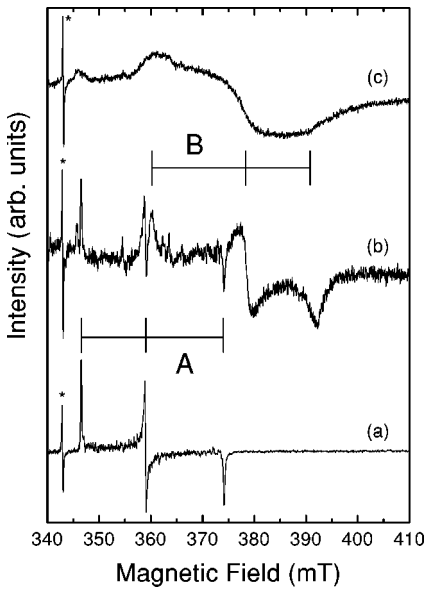

FIG. 2. Powder patterns of ESR signals observed at ~3 K in $Ca_{1-x}Y_xTiO_3$ powders with different dopant concentrations: (a) $x=10^{-4}$ with H_2-reduction at 1000 °C, (b) $x=10^{-3}$ with H_2-reduction at 800 °C, and (c) $x=10^{-2}$ in the as-prepared states. A signal attached * symbol is derived from DPPH for calibration of g values.

After H_2 reduction treatments, the donor-doped crystals with $x=10^{-4}$ and 10^{-3} became conductive, and simultaneously the complicated signals disappeared in their spectra. Instead of the disappearance of the complicated signals, four sharp signals with equivalent intensity appeared at low temperatures below ~100 K. In the case of the reduced crystal with $x=10^{-3}$, another signal with broad feature came to appear at lower temperatures below ~20 K in addition to the sharp signals. On the other hand, the non-doped sample with $x=0$ did not show any remarkable changes in the ESR spectra before and after the H_2 reduction treatments. This is probably because the non-doped sample is still insulating after the H_2 reduction treatments.

The blue colored crystals with $x=10^{-2}$, which show high electrical conductivity at room temperature in the as-prepared states, gave no signal at room temperature. However, they showed a broad signal in the temperature range below ~20 K, which is the same as the broad signal observed in the H_2-reduced crystal with $x=10^{-3}$.

To identify these signals and classify the overlapped signals, the powder patterns of the signals were measured at ~3 K. Figure 2 shows ESR signals observed for the powders of the reduced samples with $x=10^{-4}$ and 10^{-3} and the as-prepared sample with $x=10^{-2}$. It can be clearly seen that two different signals with orthorhombic symmetry, sharp and broad signals, were observed through a series of the samples with different dopant concentrations. The sharp signal was observed in the reduced samples with $x=10^{-4}$ and 10^{-3}, and the broad signal was seen in the reduced sample with $x=10^{-3}$ and the as-prepared sample with $x=10^{-2}$. Both signals were observed without illumination. Tables I and II summarize their g values estimated from the powder patterns. The sharp and broad signals are hereafter called signals A and B, and the corresponding paramagnetic centers are referred to centers A and B, respectively.

TABLE I. ESR parameters of signal A. The g-values (g), direction cosine of principal axes (l) and hyperfine coupling constants (A) evaluated from the powder pattern and single-crystal spectrum of the sample with $x=10^{-4}$ Nb concentration. The numbers denoted in the subscript express four independent signals for signal A originated from chemically equivalent centers with different orientations. The direction of x,y,z corresponds to that of the crystal coordinate a,b,c, respectively.

		x	y	z
g_{powder}		1.836	1.983	1.914
g_1		1.839	1.983	1.913
	$g_1(x)$	0.7684	0.6396	0.0201
l_1	$g_1(y)$	−0.5854	0.7153	−0.3816
	$g_1(z)$	−0.2585	0.2815	0.9241
g_2		1.836	1.985	1.916
	$g_2(x)$	0.7930	0.6054	0.0685
l_2	$g_2(y)$	−0.5865	0.7281	0.3548
	$g_2(z)$	0.1649	−0.3216	0.9324
g_3		1.835	1.987	1.911
	$g_3(x)$	0.8482	−0.5228	−0.0856
l_3	$g_3(y)$	0.5085	0.7583	0.4080
	$g_3(z)$	−0.1483	−0.3896	0.9090
g_4		1.836	1.973	1.917
	$g_4(x)$	0.8441	−0.5357	−0.0241
l_4	$g_4(y)$	0.4995	0.8017	−0.3283
	$g_4(z)$	0.1951	0.2651	0.9443
$\lvert A\rvert$ (MHz)		85	15	39

The general observations described above are equally valid for both Y-doped and Nb-doped cases. Therefore, either case is shown in the following sections.

2. Shape of signals and hyperfine structure

Figures 3(a) and 3(b) show typical single crystal ESR spectra for signal A observed in the reduced crystal with $x=10^{-4}$ and signal B in the as-prepared crystal with $x=10^{-2}$, respectively.

The paramagnetic center responsible for signal A has four independent orientations in the crystal. Therefore, four independent signals with equivalent intensity were detected in the single crystal spectra measured under an arbitary crystal orientation, as shown in the inset of Fig. 3(a). These centers are chemically equivalent because the powder patterns for

TABLE II. ESR parameters of signal B. The g-values (g) and direction cosine of principal axes (l) evaluated from the powder pattern and single crystal spectrum of the sample with $x=10^{-2}$ Nb concentration. The direction of x,y,z corresponds to that of the crystal coordinate a,b,c, respectively.

		x	y	z
g_{powder}		1.816	1.906	1.752
g		1.810	1.898	1.748
	$g(x)$	0.9836	−0.0671	−0.1674
l	$g(y)$	0.0641	0.9977	−0.0229
	$g(z)$	0.1686	0.0118	0.9856

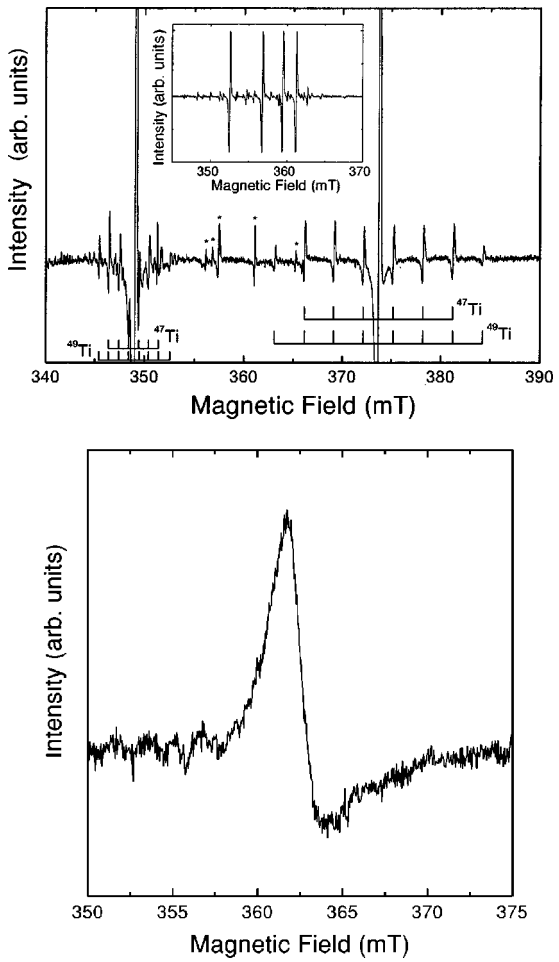

FIG. 3. ESR signals observed at ~3 K in the single crystals of $Ca_{1-x}Y_xTiO_3$, (a) $x=10^{-4}$ with H_2-reduced 1000 °C, (b) $x=10^{-2}$ in the as-prepared states. In Fig. 3(a), signals marked by * symbol are unknown and inset shows intense four signals observed at an arbitrary orientation with respect to magnetic field.

signal A resulted in a single type of signal with sharp feature (Fig. 2). The width of the signals is ~0.2 mT and fairly narrower than that of signal *B*. A pair of the signals completely overlap at a particular angle, providing only two signals in spectra as shown in Fig. 3(a). At the angle, the hyperfine structure of ^{47}Ti($I=\frac{5}{2}$,$NA=7.28\%$) and ^{49}Ti($I=\frac{7}{2}$,$NA=5.51\%$) was obviously detected. (I and NA express the nuclear spin quantum number and natural abundance, respectively.) The origin of the hyperfine structure was identified by the number of the signals split by their nuclear spins and the intensity ratio of the signals, because the hyperfine structure of the two Ti isotopes overlaps completely due to the accidental coincidence of their gyromagnetic ratio.[39] The intensity ratio of one of the inner six signals to one of the outer two signals was estimated to be ~3.0, which is close to the ideal value, ~2.8, calculated from their natural abundances.

In contrast to signal *A*, signal *B* [Fig. 3(b)] has a broad width, ~3 mT, which is more than ten times larger than that of signal *A*. The shape of the signal is distorted from the Lorentzian shape and the way of the distortion is similar to that explained by Dyson.[40,41] The large signal width and asymmetrical shape indicate that the centers of the signals are located in highly conductive materials. The skin depth where microwave penetrates was evaluated to be ~30 μm, which denotes the sample is sufficiently thicker than the skin depth. The parameter A/B that was defined by Feher and Kip in Ref. 41 was estimated from ESR spectra observed at various orientation. The value of the parameter varied between 2.0 and 3.0, and the average was 2.5. No hyperfine structure was observed for signal *B* even at low temperature, ~3 K. This might be due to the broadness of the signals, or the nature of center *B*.

3. Angular variation of resonance fields

The g value of an electron localized in paramagnetic centers is generally influenced by the spin-orbital interaction. The magnitude of the influence is reflected to the difference between the g value of the electron and that of a free electron. Therefore, the analysis of the g value provides important environmental information about the paramagnetic centers. Spin Hamiltonian, H, used in the following analysis is expressed, $H=\beta\mathbf{BgS}+\mathbf{IAS}$, where β, **B**, **g**, **A**, **S**, and **I** are a Bohr magneton, external magnetic field, g tensors, hyperfine coupling tensors, electronic and nuclear spins, respectively. For the analysis of signal *B*, only a Zeeman term was considered, because no hyperfine structure was observed for signal *B*.

Figure 4(a) shows the angular dependence of the g values for signal *A* observed in the reduced crystal with Nb concentration $x=10^{-4}$. The g^2 tensors for signal *A* were determined by the curve fitting by the least square method. The principal g values and directions of the principal axes obtained by the diagonalization of the tensors are listed in Table I. The hyperfine coupling constants for signal *A* were determined similarly with g values, construction of a A^2 tensor and its diagonalization. They are also listed in Table I.

The g values obtained for the single crystals are in reasonable agreement with those for powder samples, but a small deviation is seen between them. The deviation is probably due to some experimental errors by crystal cutting or sample setting. Since ESR spectra for powder samples are regarded as total projection of signals from numerous small crystals, the g values for powder samples are more reliable than those for single crystal samples. The directions of the principal axes are almost parallel to the directions from Ti ions to O ions coordinated in TiO_6 octahedra. Similar observation has been reported in $SrTiO_3$ by van Engelen and Henning[33] and in $BaTiO_3$ by Scharfschwerdt *et al.*[34]

Figure 4(b) shows the angular dependence of the g values for signal *B* observed in the Nb-doped crystal with $x=10^{-2}$. ESR parameters for signal *B* were estimated and they are listed in Table II. The g values resolved are in good agreement with the g values for powder samples within experimental errors. The directions of the principal axes are almost parallel to those of the crystal axes.

4. Temperature dependence of signal intensity

Figure 5 shows the temperature dependence of the signal intensity for signals *A* and *B* observed in Y- and Nb-doped samples with the dopant concentration $x=10^{-4}$ or 10^{-2}. The signal intensities in Fig. 5 are normalized by the intensity at the lowest temperature in each sample.

Signal *A* appeared below ~100 K and its intensity increased with a decrease in temperature. On the other hand,

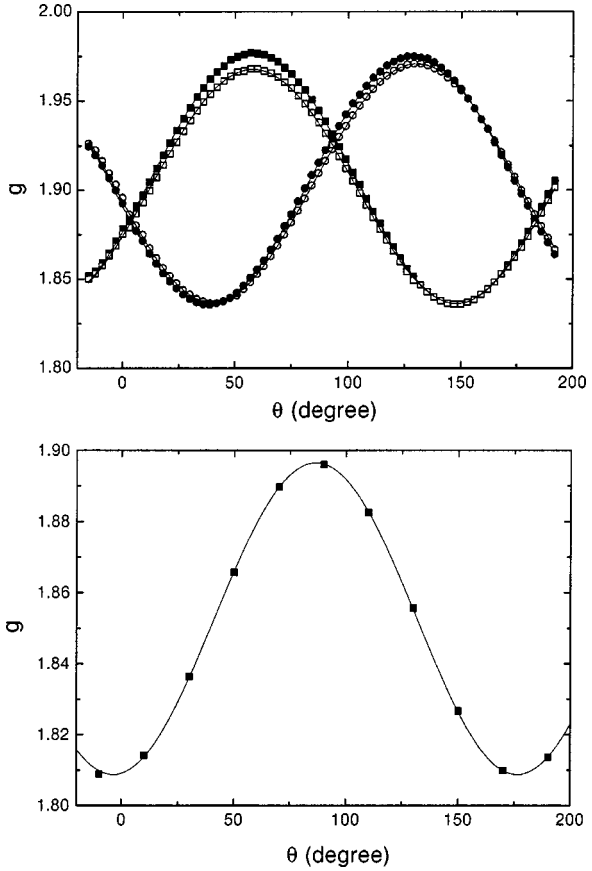

FIG. 4. Angular variation of g values for ESR signals observed in single crystals of $Ca_{1-x}Y_xTiO_3$, (a) $x=10^{-4}$ with H_2-reduced 1000 °C: signal *A*, (b) $x=10^{-2}$ in as-prepared states: signal *B*. Single crystals were rotated keeping the direction of external magnetic field in *ab* plane, and angle θ denotes the angle between the direction of magnetic field and *a* axis. Four types of symbols for signal *A* indicate four independent resonances due to chemically equivalent centers with different orientations. Solid curves are simulated by the calculation with the optimized ESR parameters.

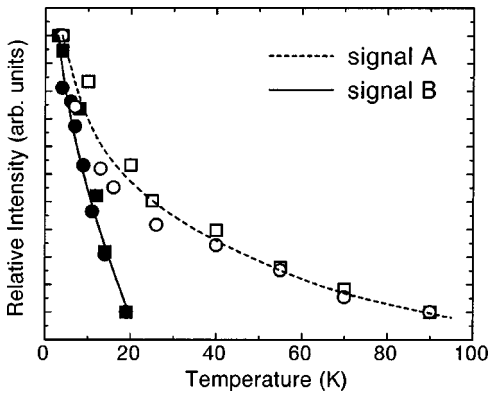

FIG. 5. Temperature dependence of relative intensity of ESR signals observed in single crystals of $Ca_{1-x}Y_xTiO_3$ and $CaTi_{1-x}Nb_xO_3$. Dashed and solid lines denote signals *A* and *B*, respectively. Symbols indicate samples in which the signals were observed: open square and circle, Y- and Nb-doped $x=10^{-4}$ with H_2-reduction at 1000 °C, solid square and circle, Y- and Nb-doped $x=10^{-2}$ in the as-prepared states, respectively.

signal *B* was observed in much lower temperature range than signal *A*. It appeared below ~20 K and gained its intensity as decreasing temperature.

The concentration of center *A* was estimated to be $\sim 3\times 10^{18}$ cm^{-3} at ~3 K in H_2-reduced samples with dopant concentration $x=10^{-4}$. On the other hand, the concentration of center *B* was evaluated to be $\sim 3\times 10^{19}$ cm^{-3} at ~3 K in the sample with dopant concentration $x=10^{-2}$. It should be noted that the concentration of center *B* is approximately ten times higher than that of center *A*.

IV. DISCUSSION

A. Assignment of ESR signals

1. Complicated signals observed in insulating samples

Several different types of signals with complicated angular dependence were observed in the insulating single crystal samples of $x=0$, 10^{-4}, and 10^{-3} in the as-prepared states. The previous study revealed that the insulating samples show *p*-type electrical conduction at high temperature and have some acceptors in the crystals.[1] As far as *p*-type electrical conduction can be observed, it is resonably assumed that the acceptors are possible paramagnetic centers rather than Y or Nb donors in the as-prepared states. Therefore, it is supposed that the acceptors are responsible for the many and complicated signals observed in the insulating samples.

The idea is experimentally supported by the observation that H_2 reduction treatment extinguished the signals observed in the samples of $x=10^{-4}$ and 10^{-3}, which became highly *n*-type electroconductive after the treatment. This observation suggests that a part of the electrons generated by the H_2 reduction are trapped at the acceptor centers, which give the complicated signals, and as a consequence the centers become no longer ESR active because of the additional trapped electrons.

To be discussed are the assignment of the signals and the determination of their origins, that is, the identification of the acceptors. From the results of electroconductive properties of the samples reported in the previous paper, two possible origins for the acceptors were proposed: one is Al^{3+} impurity defects at Ti^{4+} sites, and the other is oxygen excess mainly derived from the deviation of the cation ratio, Ca/Ti, from the stoichiometry. In both cases, nonstoichiometry of oxygen plays an important role in the compensation for donors and *p*-type electrical conduction.

In the present ESR measurements, Al^{3+} centers at Ti^{4+} sites were not observed for any samples, nevertheless its concentration, ~1000 ppm, is high enough for the detection of the centers. In addition, the signals derived from the oxygen excess could not be separated or extracted from the complicated signals. Although Fe-related signals were observed, the concentration of Fe ions in the samples is less than 100 ppm, which is one order of magnitude lower than that of Al ions. Consequently, as stated in the results section, the assignment of the many signals was unfortunately suspended owing to their complexity.

2. Signal A

Signal *A* shows orthorhombic symmetry and its g values are smaller than that of a free electron, $g_e=2.0023$. The negative shift, $g-g_e$, indicates that signal *A* originates from

an electron-trapped-type paramagnetic center. Signal *A* was observed at relatively high temperature and its signal width is rather narrow in comparison with signal *B*. These observations demonstrate that an electron trapped at center *A* is considerably localized and the energy level of the center is relatively deep from the bottom of the conduction band. The detection of hyperfine structure due to a single Ti isotope, ^{47}Ti, or ^{49}Ti, evidenced that an electron trapped at center *A* is localized fairly close to a Ti nucleus. Therefore, signal *A* can be assigned to a Ti^{3+} paramagnetic center, at which an electron is tightly and deeply trapped with an influence of Ti nuclear spin.

This assignment is further supported by another observation that the direction of the principal axes nearly coincides with that of the direction cosine of Ti-O vectors in the TiO_6 octahedra. In addition, signal *A* consists of four signals indicating the presence of four chemically equivalent sites in the crystal, which is consistent with the fact that $CaTiO_3$ has four independent Ti sites crystallographically.

To proceed to more detailed discussions of signal *A*, let us consider the origins of electrons trapped at Ti^{3+} centers. Sharp signals analogous to signal *A* were observed in H_2-reduced pure $SrTiO_3$ by van Engelen and Henning.[33] The signals they observed have *g* values almost the same as those of signal *A* and they observed hyperfine structure of Ti isotopes simultaneously. Therefore, the centers for their signals were supposed to be identical with center *A*. Since no dopant is included in the sample they used, oxygen vacancies introduced by the reduction treatment are the most reasonable origin of the trapped electrons. They concluded that Ti^{3+} is located at a Sr site. However, the conclusion seems to be inappropriate for the present case under the consideration of coulombic interaction at a Ti or Sr/Ca site and their ionic radii.

Recently, oxygen vacancies in $BaTiO_3$ were intensively studied using ESR techniques by Scharfschwerdt *et al.*[34] Three types of signals were observed in their samples and three corresponding models were proposed. Although accuracy in angular analysis in our experiments is not as high as that in their experiments, $Ti^{3+}-V_o$ centers or isolated Ti^{3+} centers they proposed seems to be a candidate for center *A*. However, *g* values of the signals they estimated for these centers are quite different from those for signal *A*, and hyperfine structure concerning to Ti isotopes were not detected in their studies. If the difference in the *g* values may be explained merely by the crystal distortion of $CaTiO_3$, similar signals should be observed in $SrTiO_3$ and $BaTiO_3$ except $CaTiO_3$, because former two materials have almost ideal perovskite crystal structure even at low temperatures. However, similar signals were observed between $CaTiO_3$ and $SrTiO_3$, not $SrTiO_3$ and $BaTiO_3$. Therefore, the detailed model for center *A* is still open question and further accurate analysis is needed for its determination.

To summarize the assignment of signal *A*, signal *A* results from Ti^{3+} center, at which an electron is tightly and deeply localized. The localized electrons are generated by the formation of oxygen vacancies but the position of the oxygen vacancies is unknown so far. However, the location of the oxygen vacancies is expected to be in the vicinity of the Ti^{3+} centers if not at the neighbor sites.

3. Signal B

Signal *B* has a larger negative *g*-shift than signal *A*, showing that the origin of signal *B* is an electron-trapped-type center. However, different from signal *A*, signal *B* was observed as a signal with a distorted shape at lower temperatures and its signal width is fairly broad. The temperature dependence of its signal intensity implies that the energy level of the center for signal *B* is quite shallow from the bottom of the conduction band, and its broad signal width may suggest that electrons are localized not tightly but loosely with a spatial spread over several ions around the central ions.

The shape of signal *B* is dysonian, which is frequently observed in metals or graphite with high conduction electron concentration. The distortion of the signal shape originates from the skin effect by conduction electrons, and the dysonian absorption observed in metals or graphite is assigned to the conduction electrons. Since the samples in which signal *B* was observed have high electrical conductivity with metallic behavior, conduction electrons in them cause the dysonian distortion of signal *B*. However, it should be noted that signal *B* showed large temperature dependence of signal intensity at low temperatures. Moreover, the average value of the parameter A/B for signal *B* was 2.5, which is close to the value, 2.7, predicted by Feher and Kip for stationary paramagnetic centers that are distributed throughout the volume and give a Lorentzian type of signal. Therefore, signal *B* should be assigned to quite shallow electron-trapped-type centers rather than free delocalized electrons in the present case.

It is not anticipated that oxygen vacancies are responsible for the signal, because the samples were not treated in H_2 reducing atmosphere. Although the donor centers, Y^{2+} or Nb^{4+} centers, were not detected even at $\sim$3 K, signal *B* may be tentatively attributed, from the following discussion, to donor-related centers at which some of the conduction electrons are loosely trapped in a large space including a few ions.

If a hydrogen-atom-like model is applied to the donors, an orbital for the trapped electron is expected to have relatively large radius and the binding energy would be small because the static dielectric constant of $CaTiO_3$ is large. (The radius and binding energy are estimated to be $\sim$20 Å and 1 meV, respectively, on the assumption that $m^*=\sim 10m_0^3$, $\epsilon_r=\sim 350$,[42] where m^*, m_0, and ϵ_r denote effective mass, mass of electron and relative dielectric constant, respectively. If polarizing effects are included, the radius will decrease and the energy will increase somewhat because of an increase in the effective mass.) This model seems to describe the present electron-trapped-type centers semiquantitatively because the binding energy estimated corresponds to the energy of $\sim$10 K, which is close to the temperature at which electrons start to be localized at center *B*. According to the model, an electron trapped at center *B* moves around $\sim$20 Å away from its central ion, supposedly the donor ion. Therefore, it seems to be inevitable that hyperfine structure due to donor nucleus was not observed and the feature of signal *B* is almost the same in Y- and Nb-doped samples.

In summary, signal *B* was tentatively assigned to the donor center that traps a conduction electron, at which an electron is loosely localized moving around a donor at several Å

distance from its center. Although no obvious evidence to determine the central ion is available so far, a donor ion, Y or Nb ion, is most probable for the central ion under the consideration of coulombic interaction.

B. Correlation between electrical conductivity and ESR centers

1. Signal A

The H_2-reduced samples with $x=10^{-4}$ Y or Nb concentration show metallic behavior at low temperatures, and no remarkable change was observed in electrical conductivity. Although only signal *A* appears in the H_2-reduced samples and center *A* traps an electron blow ~100 K, no relationship was found between temperature dependence of electrical conductivity and that of signal intensity.

Signal *A* was observed in H_2-reduced crystals with Y or Nb concentration $x=10^{-4}$ or 10^{-3}, and the density of electrons for signal A in the reduced samples with $x=10^{-4}$ was found to be $\sim 3\times 10^{18}$ cm^{-3} at low temperatures. The ideal carrier density in nominally $x=10^{-4}$ samples is estimated to be $\sim 2\times 10^{18}$ cm^{-3} assuming that each donor completely generates a single electron. The ideal carrier density is comparable to the electron density for signal *A*. However, the carrier density experimentally estimated by the Hall measurements for the samples at room temperature was a few order of magnitude lower than that for signal *A*.[1] Therefore, these observations suggest that electrons trapped at center A may not act as conduction electrons at high temperature.

It was observed that the intensity of signal *A* decreased with an increase in temperature. Probably, this temperature dependence of the signal intensity does not mean the release or delocalization of the trapped electrons. The dependence primarily originates from a decrease in the relaxation time, as observed in Ti^{3+}-doped oxides such as $Al_2O_3:Ti, LiNbO_3:Ti, YAlO_3:Ti$ and so on.[43–45] Judging from the metallic behavior of these samples, the conduction electrons in the samples seems to originate from another center, supposedly quite low density of center *B*, which is undetectable by ESR technique due to the small amount.

2. Signal B

The as-prepared sample with $x=10^{-2}$ Y or Nb concentration shows metallic behavior at low temperatures down to ~25 K. However, re-examination of electrical conductivity at low temperatures clarified that semiconducting behavior appears below ~25 K. Since the electrical conductivity is generally defined by the product of the carrier mobility and density, the decrease in the conductivity results from the decrease of the carrier mobility or density. Suppose that the temperature dependence of Hall mobility in $SrTiO_3$ (Ref. 46) is similar to that in $CaTiO_3$, that is, the temperature dependence of Hall mobility in $CaTiO_3$ is quite small below ~10 K, the decrease in the electrical conductivity primarily originates from the decrease in the carrier density.

Intensity of signal *B* observed in the samples increases with a decrease in temperature below ~20 K. Its temperature range almost coincides with the temperature range in which the electrical conductivity or carrier density decreases. Therefore, it is considered that electrons trapped at the centers are probably some of the conduction electrons, and the decrease in the electrical conductivity is due to capture of electrons by center *B*.

The concentration of the electrons trapped at center *B* was roughly estimated to be $\sim 3\times 10^{19}$ cm^{-3} in the $x=10^{-2}$ samples without consideration of the skin effect. If the effect is taken into consideration, the concentration would be higher than the magnitude above. The ideal carrier concentration for nominally $x=10^{-2}$ samples is $\sim 2\times 10^{20}$ cm^{-3}. The concentration of electrons trapped at center *B* is some tens percent of the ideal carrier concentration. On the other hand, the carrier density for the samples at ~20 K estimated by the Hall measurements previously was $\sim 8\times 10^{18}$ cm^{-3}, which is approximately four times smaller than the concentration of center *B*. The reason for these discrepancies is unknown so far. It implies, however, that a certain center undetectable by ESR may cause some compensation of carriers, and the center would be related to oxygen excess that was discussed in the previous paper.[1]

The sample is still highly conductive even at 1.6 K. This result suggests that the center *B* forms fairly shallow energy level, from the bottom of the conduction band. Since metallic behavior was observed at high temperatures, the level seems to turn into a band-like state partially overlapping with the bottom of the conduction band. Since the conduction band of $CaTiO_3$ mainly consists of a Ti 3d band, the state for center *B* at high temperature will be expressed as a hybridized state between orbitals of donors and Ti $3d$ orbitals.

V. CONCLUSION

ESR measurements were carried out on $Ca_{1-x}Y_xTiO_3$ and $CaTi_{1-x}Nb_xO_3$ single crystals to clarify the carrier generation and compensation mechanism in the materials. Moreover, electrical conductivity of the crystal with $x=10^{-2}$ was measured down to 1.6 K to re-examine the electroconductive behavior at low temperatures. From the analysis of the results, three assignments were concluded as follows with respect to the signals observed.

(1) Several types of signals were observed in the insulating single crystals of $x=0$, 10^{-4}, and 10^{-3} in the ESR measurements. Since the signals observed in the insulating crystals disappeared after H_2 reduction treatments, which cause the generation of electrons, it was suggested that the paramagnetic centers for these signals are derived from some acceptors.

(2) Sharp signals were observed below ~100 K in the reduced samples with low dopant concentration, and they were assigned to Ti^{3+} centers related to oxygen vacancies. Sharp shapes of the signals, observation of the hyperfine structures of ^{47}Ti and ^{49}Ti, and the directions for the principal axes of the *g* tensor imply that the electrons trapped at the Ti^{3+} centers are deeply and tightly localized at low temperatures.

(3) A broad signal was observed below ~20 K in the sample with high dopant concentration. Since a correlation between the electrical conductivity and signal intensity was found in the low temperature range, the signal was tentatively assigned to a donor-related center, at which some conduction electrons are loosely trapped over several Ti ions

around the central donors. The center forms a fairly shallow energy level from the bottom of the conduction band at low temperature, while it seems to change into a band-like state with a Ti 3d band at high temperature resulting in a metallic electroconductive behavior.

ACKNOWLEDGMENTS

We thank Professor M. Itoh of Tokyo Institute of Technology for his support in electrical conductivity measurements.

*Now with R&D Center, HOYA Corp., 3-3-1 Musashino, Akishima 196-8510.

[1] K. Ueda, H. Yanagi, H. Hosono, and H. Kawazoe, Phys. Rev. B **56**, 12 998 (1997).

[2] I.S. Kim, M. Ito, and T. Nakamura, J. Solid State Chem. **101**, 77 (1992).

[3] H.P.R. Frederikse, W.R. Thurber, and W.R. Hosler, Phys. Rev. **134**, A442 (1964).

[4] H. Yamada and G.R. Miller, J. Solid State Chem. **6**, 169 (1973).

[5] N.G. Error and D.M. Smyth, J. Solid State Chem. **24**, 235 (1978).

[6] T. Murakami, M. Nakahara, T. Miyashita, and S. Ueda, J. Am. Ceram. Soc. **56**, 291 (1973).

[7] K. Ueda, H. Yanagi, H. Hosono, and H. Kawazoe, J. Phys.: Condens. Matter **11**, 3535 (1999).

[8] K. Ueda, H. Yanagi, R. Noshiro, H. Hosono, and H. Kawazoe, J. Phys.: Condens. Matter **10**, 3669 (1998).

[9] P. Pertosa and F.M. Michel-Calendini, Phys. Rev. B **17**, 2011 (1978).

[10] A.H. Kahn and A.J. Leyendecker, Phys. Rev. **135**, A1321 (1964).

[11] T.F. Soules, E.J. Kelly, D.M. Vaught, and J.W. Richardson, Phys. Rev. B **6**, 1519 (1972).

[12] L.F. Mattehiss, Phys. Rev. B **6**, 4718 (1972).

[13] F.L. Battye, H. Höchst, and A. Goldmann, Solid State Commun. **19**, 269 (1976).

[14] B. Reihl, J.G. Bednorz, K.A. Mler, Y. Jugnet, G. Landgren, and J.F. Morar, Phys. Rev. B **30**, 803 (1984).

[15] Y. Tezuka, S. Shin, T. Ishii, T. Ejima, S. Suzuki, and S. Sato, J. Phys. Soc. Jpn. **63**, 347 (1994).

[16] M. Cardona, Phys. Rev. A **140**, A651 (1965).

[17] D. Bäuerle, W. Braun, V. Saile, G. Sprüssel, and E.E. Koch, Z. Phys. B **29**, 179 (1978).

[18] A. Frova and P.J. Boddy, Phys. Rev. **153**, 606 (1967).

[19] E. Possenriede, P. Jacobs, and O.F. Schirmer, J. Phys.: Condens. Matter **4**, 4719 (1992).

[20] E. Possenriede, O.F. Schirmer, and H.J. Donnerberg, Ferroelectrics **92**, 245 (1989).

[21] B.W. Faughnan, Phys. Rev. B **4**, 3623 (1971).

[22] Th.W. Kool and M. Glasbeek, J. Phys.: Condens. Matter **5**, 361 (1993).

[23] E.S. Kirkpatrik, K.A. Müller, and R.S. Rubins, Phys. Rev. A **135**, A86 (1964).

[24] H. Unoki and T. Sakudo, J. Phys. Soc. Jpn. **23**, 546 (1967).

[25] Th.W. Kool, H.J. de Jong, and M. Glasbeek, J. Phys.: Condens. Matter **6**, 1571 (1994).

[26] A. Logendijk, R.J. Morel, M. Glasbeek, and J.D.W. van Voorst, Chem. Phys. Lett. **12**, 518 (1972).

[27] K.A. Müller, W. Berlinger, and R.S. Rubins, Phys. Rev. **186**, 361 (1969).

[28] M. Nakahara, and T. Murakami, J. Appl. Phys. **45**, 3795 (1974).

[29] T. Takeda, J. Phys. Soc. Jpn. **24**, 533 (1968).

[30] T.C. Ensign and S.E. Stokowski, Phys. Rev. B **1**, 2799 (1970).

[31] O.F. Schirmer, W. Berlinger, and K.A. Müller, Solid State Commun. **18**, 1505 (1976).

[32] T. Varnhorst, O.F. Schirmer, H. Kröse, and R. Scharfschwerdt, Phys. Rev. B **53**, 116 (1996).

[33] P.P.J. van Engelen and J.C.M. Henning, Phys. Lett. **25A**, 733 (1967).

[34] R. Scharfschwerdt, A. Mazur, O.F. Schirmer, H. Hesse, and S. Mendricks, Phys. Rev. B **54**, 15 284 (1996).

[35] E. Possenriede, H. Kröse, T. Varnhorst, R. Scharfschwerdt, and O.F. Schirmer, Ferroelectrics **151**, 199 (1994).

[36] T. Takeda and A. Watanabe, J. Phys. Soc. Jpn. **21**, 267 (1966).

[37] P.H. Zimmermann, Phys. Rev. **8**, 3917 (1973).

[38] S. Sasaki, C.T. Prewitt, J.D. Bass, and W.A. Schulze, Acta Crystallogr., Sect. C: Cryst. Struct. Commun. **43**, 1668 (1987).

[39] C.D. Jeffries, Phys. Rev. **92**, 1262 (1953).

[40] F.J. Dyson, Phys. Rev. **98**, 349 (1955).

[41] G. Feher and A.F. Kip, Phys. Rev. **98**, 337 (1955).

[42] A. Linz and K. Herrington, J. Chem. Phys. **28**, 824 (1958).

[43] N.E. Kask, L.S. Kornieko, T.S. Mandel'shtam, and A.M. Prokhorov, Fiz. Tverd. Tela (Lenningrad) **5**, 2306 (1963) [Sov. Phys. Solid State **5**, 1677 (1964)].

[44] G. Corradi, I.M. Zaritskii, A. Hofstaetter, K. Polgár, and L.G. Rakitina, Phys. Rev. B **58**, 8329 (1998).

[45] M. Yamaga, T. Yoshida, B. Henderson, K.P. O'Donnell, and M. Date, J. Phys.: Condens. Matter **4**, 7285 (1992).

[46] O.N. Tufte and P.W. Chapman, Phys. Rev. **155**, 796 (1967).